Mineralogy and Petrology (2003) 79: 285–307
DOI 10.1007/s00710-003-0013-5

Mineralogy and Petrology

Telluride mineralogy of the low-sulfidation epithermal Emperor gold deposit, Vatukoula, Fiji

D. W. Pals and **P. G. Spry**

Department of Geological and Atmospheric Sciences, Iowa State University, Ames, Iowa, U.S.A.

Received January 14, 2003; revised version accepted June 26, 2003
Editorial handling: E. F. Stumpfl

Summary

The epithermal, low sulfidation Emperor gold telluride deposit in Fiji, hosted by Late Miocene-Early Pliocene shoshonitic rocks, is spatially related to a low-grade porphyry Cu system on the western flank of the Tavua Caldera. Gold is largely in the form of ''invisible'' gold in arsenian pyrite but 10 to 50% of gold is in the form of precious metal tellurides. Gold mineralization occurs in steeply dipping dikes and faults, flat-dipping structures ($<45°$), referred to locally as ''flatmakes,'' and at the intersection of two or more structures referred to as ''shatter zones.'' Petrographic, electron microprobe, and scanning electron microscope analyses of ores from some of the more recently discovered orebodies, Matanagata, Matanagata East, and R1 reveal that tellurium-bearing minerals, sylvanite, calaverite, krennerite, petzite, hessite, coloradoite, melonite, native tellurium, and rare benleonardite, formed during various hydrothermal stages, hosted in quartz, and to a lesser extent arsenian pyrite and tetrahedrite group minerals. Sylvanite followed by krennerite are the two most common tellurides in these orebodies. These tellurides show no systematic spatial distribution within flatmakes but there appears to be a higher concentration of tellurides where the flatmake intersects steep structures. Gold-rich tellurides preceded the formation of silver-rich tellurides and were constrained at 250 °C in $\log f S_2$ and $\log f Te_2$ space at -12.7 to -10.1 and -9.4 to -7.8, respectively, based on sulfide and telluride stabilities, and the composition of sphalerite. Ore forming components, such as Au, Ag, Te, Cu, V, and S, were likely derived from Late Miocene-Early Pliocene monzonites in and adjacent to the Tavua caldera.

Introduction

Epithermal gold telluride deposits constitute some of the world's largest sources of gold and occur in igneous rocks of alkaline (e.g., Cripple Creek, Colorado,

Thompson et al., 1985) to calc-alkaline affinity [e.g., Săcărîmb, Romania, *Alderton* and *Fallick* (2000)]. Included in the group of epithermal deposits genetically related to alkaline igneous rocks is the Emperor gold–silver telluride deposit, Fiji, which contains approximately 10 Moz of Au. The Emperor deposit, hosted by Tertiary shoshonitic rocks, occurs on the western flank of the Tavua Caldera in north-central Viti Levu (Fig. 1). Although much of the gold in the Emperor deposit occurs as ''invisible'' gold in pyrite (*Pals* et al., 2003), 10 to 50% of the visible precious metal budget of the ore is in the form of precious metal tellurides, with

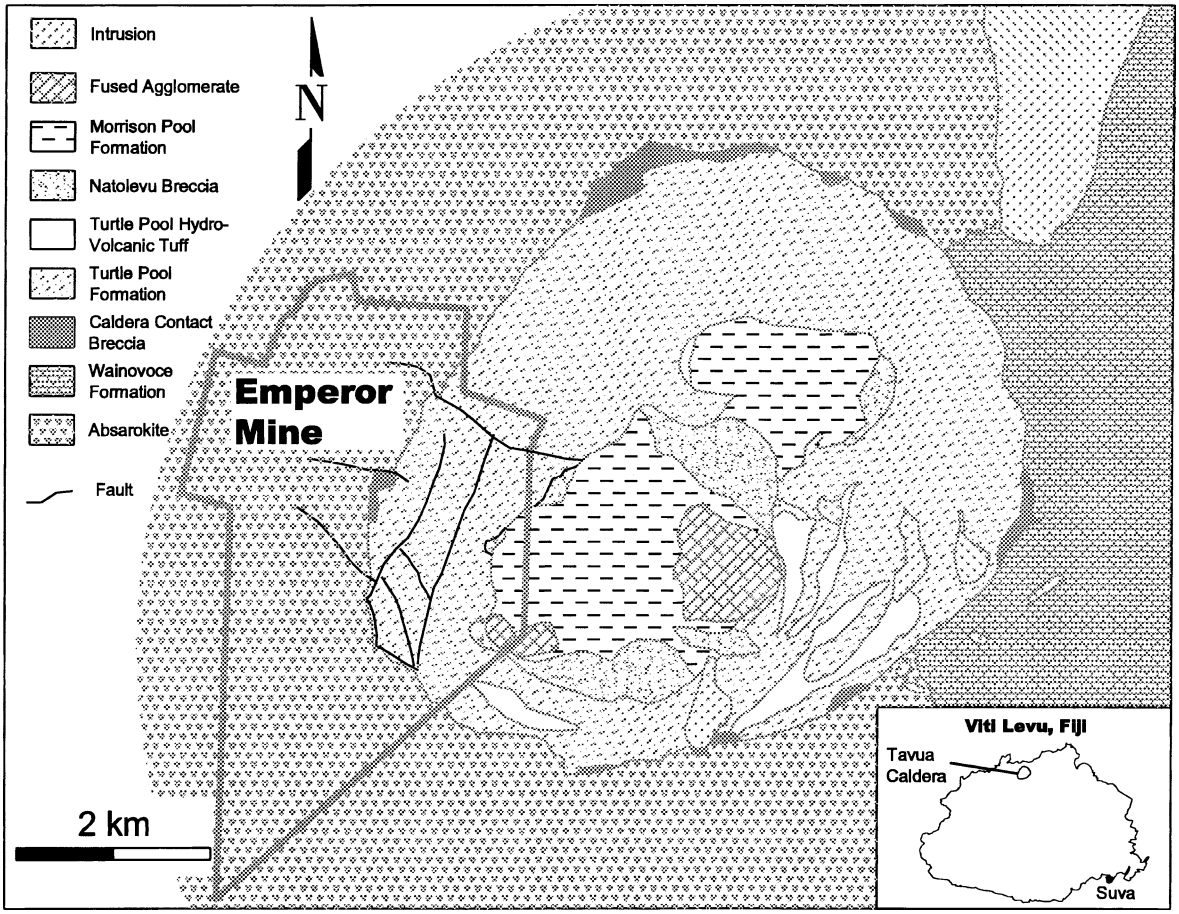

Fig. 1. Generalized geological map of the Tavua Caldera, Fiji (modified after *Eaton* and *Setterfield*, 1993; *Begg*, 1996; and *Olubas*, 1998). Outlined area represents tenements leased by Emperor Gold Mines, Ltd. The lithologies associated with each formation or rock type are as follows with the compositions in brackets (*Setterfield* et al., 1991; *Begg*, 1996): Wainovoce Formation – aa lava flows, debris flows and minor airfall tuffs (shoshonite and plagioclase absarokite); Caldera Contact Breccia – mass flow deposits (heterolithic); Turtle Pool Hydro-Volcanic Tuff – lava flows, lacustrine sediments, lapilli tuffs (shoshonite); Natolevu Breccia – mass flow deposits (heterolithic); Morrisons Pool Formation – lava flows, subaerial pyroclastic rocks, minor sediments (banakite); Intrusion – Rabulu Gap Intrusive (monzonite)

native gold in subordinate amounts. The average gold grade since commencement of mining in the early 1930s has been about 9 g/t but with localized bonanza grades in excess of 2,000 g/t.

The telluride mineralogy of the Emperor deposit has been described for the central and western parts of the deposit (e.g., *Stillwell*, 1949; *Stumpfl*, 1970; *Forsythe*, 1967, 1971; *Markham*, 1960; *Ahmad* et al., 1987; *Kwak*, 1990), however, the distribution and nature of the tellurides in the eastern portion of the deposit have received minimal attention. Paragenetic studies have been restricted to the central and western parts of the deposit and have led to conflicting interpretations. In a detailed mineralogical and geochemical study of ''flatmakes'' (a local term for flat-dipping structures ($<45°$)), in the central part of the mine, *Ahmad* et al. (1987) proposed eight stages (I–VIII) of vein growth at the Emperor deposit, two of which (stages II and IV) contained tellurides, whereas *Begg* (1996) considered the stages of vein growth to be vein cycles whereby each cycle represented a separate hydrothermal event in a given flatmake. According to *Begg* there may be some correlation among growth cycles in flatmakes and steep shears, but he also proposed there may be as many as forty different growth cycles during the

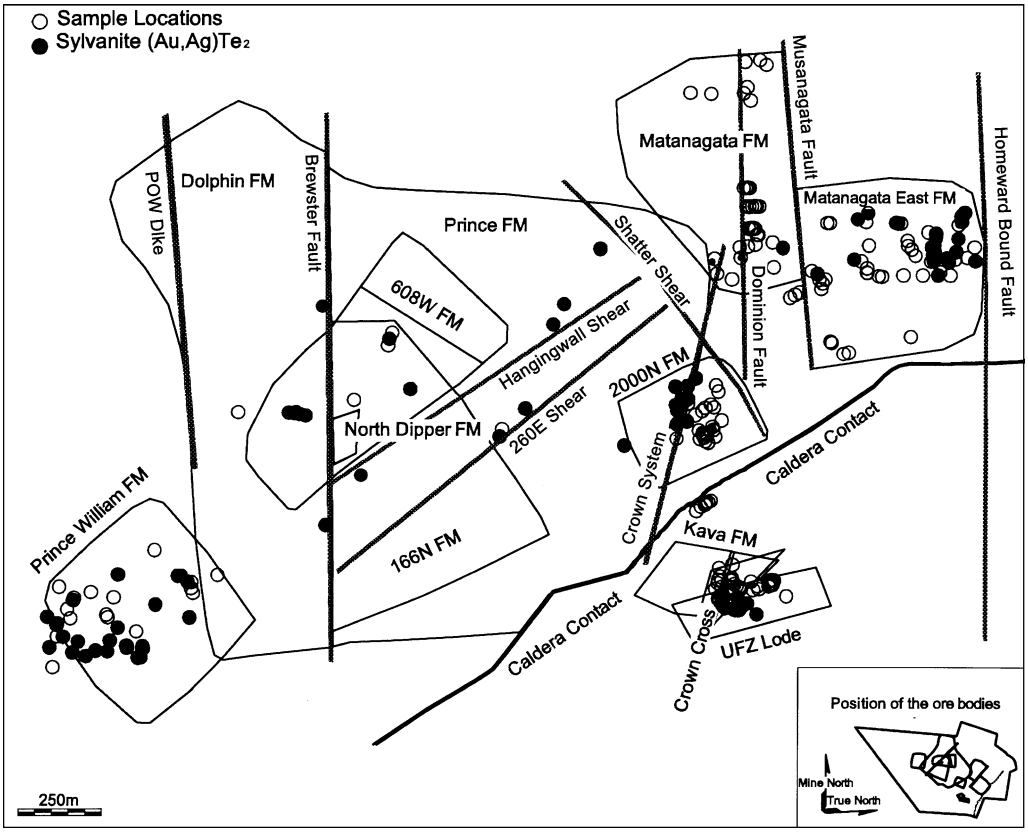

Fig. 2. Plan-view of the ore bodies at the Emperor gold mine projected to the surface. Open circles indicate sample locations. Filled circles show sylvanite occurrences from this study, *Begg* (1996), and *Ahmad* et al. (1987). *FM* Flatmake

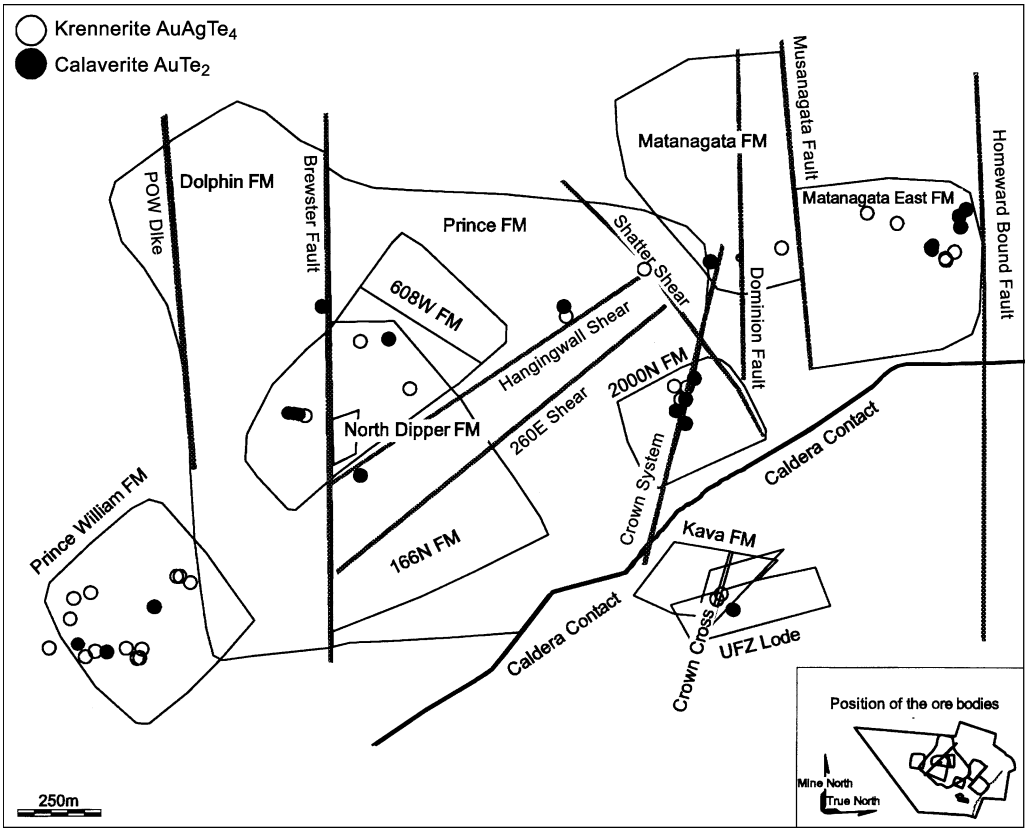

Fig. 3. Plan-view of the ore bodies at the Emperor gold mine projected to the surface. Open circles indicate krennerite locations whereas filled circles mark the locations of calaverite occurrences from this study, *Begg* (1996), and *Ahmad* et al. (1987)

hydrothermal ore-forming event at Emperor, implying there may be minimal, if any correlation.

In view of the fact that the eastern lodes (e.g., Matanagata East, Matanagata, and R1) provide the majority of the currently mined ore and given that paragenetic and mineralogical studies have concentrated on the western and central orebodies, the aims of the present study are to determine the identity, spatial distribution and paragenesis of tellurides within the eastern orebodies, and to evaluate the conditions of formation of tellurides in the Emperor ore-forming system. Some attention has also been directed towards determining the mineralogy of other flatmakes (mainly, 2000N and Prince William) for comparative purposes (Figs. 2 and 3).

Geological setting

The regional and local geology is summarized here but is described in detail by *Colley* and *Flint* (1995), *Begg* (1996), and *Begg* and *Gray* (2002). The Fiji islands are situated on a prominent offset between the west-dipping Tonga-Kermadec

subduction zone to the east and the east-dipping Vanuatu subduction zone to the west. The offset marks a broad zone of spreading and transform faulting to accommodate the shape of the subduction zone. During the mid-late Miocene, the New Hebrides island arc, the Fiji platform, and the Lau-Tonga ridge were considered to be one continuous island arc (*Rodda*, 1993). This arc system was active from the early Eocene to the middle Miocene (*Gill* and *McDougall*, 1973). Collision of the arc with overthickened oceanic crust of the Melanesian border plateau is thought to be the mechanism that halted the general ENE–WSW subduction trend (*Gill* and *Whelan*, 1989).

The Late Miocene-Early Pliocene Ba Volcanic Group dominates the northern half of Viti Levu and is composed primarily of shoshonitic lavas. The formation of the Ba Volcanic Group is associated with at least three volcanic centers, the largest of which, the Tavua Volcano, occurs along the regional Viti Levu lineament, and immediately adjacent to the Emperor gold deposit (*Begg*, 1996). The Tavua Volcano, which covers an area of about 1,300 km^2, formed at ~4.5 Ma (*Begg*, 1996). Caldera collapse caused tilting of approximately 10° and resulted in extension in the southwestern portions of the caldera where the Emperor deposit is located. Details of the sequence of events associated with caldera collapse are described in detail by *Setterfield* et al. (1991) and *Begg* (1996). Petrological and geochemical studies of alkaline volcanic rocks associated with the Tavua Volcano by *Rogers* and *Setterfield* (1994) showed that the volcano grades upwards from subaqueous, to subaerial flows with lesser airfall tuff and volcanic breccia. The subaerial flows are composed mostly of absarokite, plagioclase absarokite, shoshonite, and rare banakite flows. The central part of the volcano is infilled with shoshonitic lavas and sediments of the Morrison Pool Formation and is overlain by banakitic sediments of the Turtle Pool Formation. The Caldera Contact Breccia is a sequence of heterolithic debris flows, which contains mafic to intermediate fragments in a sandy matrix along the margins of the Tavua Caldera. Monzonitic stocks occur in the center of the Tavua Caldera (*Eaton* and *Setterfield*, 1993) but also occur in the ore zone (*Begg*, 1996).

Rogers and *Setterfield* (1994) proposed that the alkaline lavas were erupted during the breakup of the Vanuata-Fiji-Tonga arc and evolved from absarokite through shoshonite to banakite. Major, trace, and radiogenic isotope are consistent with these rocks having formed by high degrees of melting during subduction.

Pre-epithermal, low-grade, porphyry Cu-style mineralization occurs along the margins of the Tavua Caldera associated with steep caldera faults spatially related to epithermal gold mineralization. The most common styles of alteration associated with the porphyry Cu-style mineralization are potassic, propylitic, and phyllic with minor skarns (*Begg*, 1996). Epithermal gold mineralization occurs in and adjacent to steeply dipping dikes and faults, ''flatmakes,'' and ''shatter zones.'' Flatmakes are generally hosted in basalt overlain by ash-rich units whereas the R1 lodes occur in andesites overlain by tuffaceous units in the Tavua Caldera. The porphyry-style and epithermal mineralization were essentially synchronous as indicated by ^{40}Ar–^{39}Ar whole-rock and mineral ages of 3.89 ± 0.05 Ma (*Begg*, 1996; *Begg* and *Gray*, 2002).

Epithermal lodes are often bonanza zones that are composed of fine-grained tellurides associated with quartz, adularia, dolomite, arsenian pyrite, roscoelite, and

wall-rock fragments on the margins of generally gold-free, medium-grained quartz, adularia, and rare barite (*Ahmad* et al., 1987; *Begg*, 1996). The veins show open-spaced textures with crustiform cockscomb quartz. In places, rare coarse-grained telluride crystals project into vugs. Minor amounts of tellurides also occur in a zone up to 10 cm wide of potassic alteration composed of fine-grained quartz, adularia, dolomite, pyrite, ilmenite, chlorite, roscoelite, and minor sulfides, sulfosalts, and oxides on the margins of the veins. With increasing distance from the veins, a spotted pale green-gray carbonatized, gold-free zone consisting of dolomite, quartz, chlorite, adularia, pyrite, ilmenite is common. The vein in addition to the potassic and carbonate alteration zones are superimposed on propylitic alteration composed primarily of chlorite, calcite, and magnetite. A common feature of the flatmakes, which has been described by *Ahmad* et al. (1987) and *Begg* (1996), is for the alteration zones to be symmetrical about the vein with the tellurides, sulfides, quartz, and adularia to be more common on the footwall side. The hanging wall side of the vein may only contain quartz and carbonate. Although *Ahmad* et al. (1987) suggested that this feature may be the result of gravitational setting of heavier particles, *Begg* (1996) suggested that vapor bubbles produced during boiling may have prevented the growth of some of the mineral particles including the tellurides.

Fluid inclusion studies of the Emperor deposit by *Ahmad* et al. (1987), *Kwak* (1990), *Eaton* and *Setterfield* (1993), *Begg* (1996), and *Poliquin* (1996) show that early porphyry-style mineralization formed at 200° to 400 °C from a locally boiling, low-salinity fluid (1 to 6 wt% NaCl equiv), with a subordinate moderately saline fluid (~14 wt% NaCl equiv). *Ahmad* et al. (1987) and *Begg* (1996) demonstrated that homogenization temperatures (T_h) of epithermal mineralization range from 150° to 250 °C and that there was a general decline in T_h from 250 °C to approximately 180 °C during deposition of various flatmakes. *Begg* (1996) obtained salinities for epithermal ranging from 1 to 15 wt% NaCl equiv. (mean = ~8.5 wt% NaCl equiv) whereas *Ahmad* et al. (1987) reported a narrower range 4.6 to 7.1 wt% NaCl equiv (mean = ~5.5 wt% NaCl equiv).

Electron microprobe analyses

Polished-thin sections of ore samples were examined with an Olympus BK-40 dual reflected-transmitted light petrographic microscope whereas native elements, tellurides, sulfides, and sulfosalts in selected samples were analyzed with an ARL-SEMQ electron microprobe to determine their compositions. Standards used for the electron microprobe for native elements, tellurides, sulfides, and sulfosalts, were pure metals (for Ag, Au, Cu, and Te), natural cinnabar (HgS) for Hg and galena (PbS) for Pb, and the following synthetic minerals: matildite ($AgBiS_2$) for Bi, stibnite (Sb_2S_3) for Sb, orpiment (As_2S_3) for As, sudovikovite ($PtSe_2$) for Se, sphalerite (ZnS) for Zn, pyrrhotite ($Fe_{0.939}S$) for Fe and S. The ARL-SEMQ electron microprobe employed the PRSUPR data-reduction procedure of *Donovan* et al. (1992). Operating conditions for the microprobe included an accelerating voltage of 20 kV and a sample current of 10 nA. The electron beam was focused to 2 microns in diameter for all analyses. Some of these samples were also analyzed with a Hitachi S-2460N reduced-vacuum scanning electron microscope (SEM) equipped with

Table 1. *Paragenetic sequence of minerals from the Emperor gold deposit, Fiji (modified after* Ahmad *et al., 1987)*

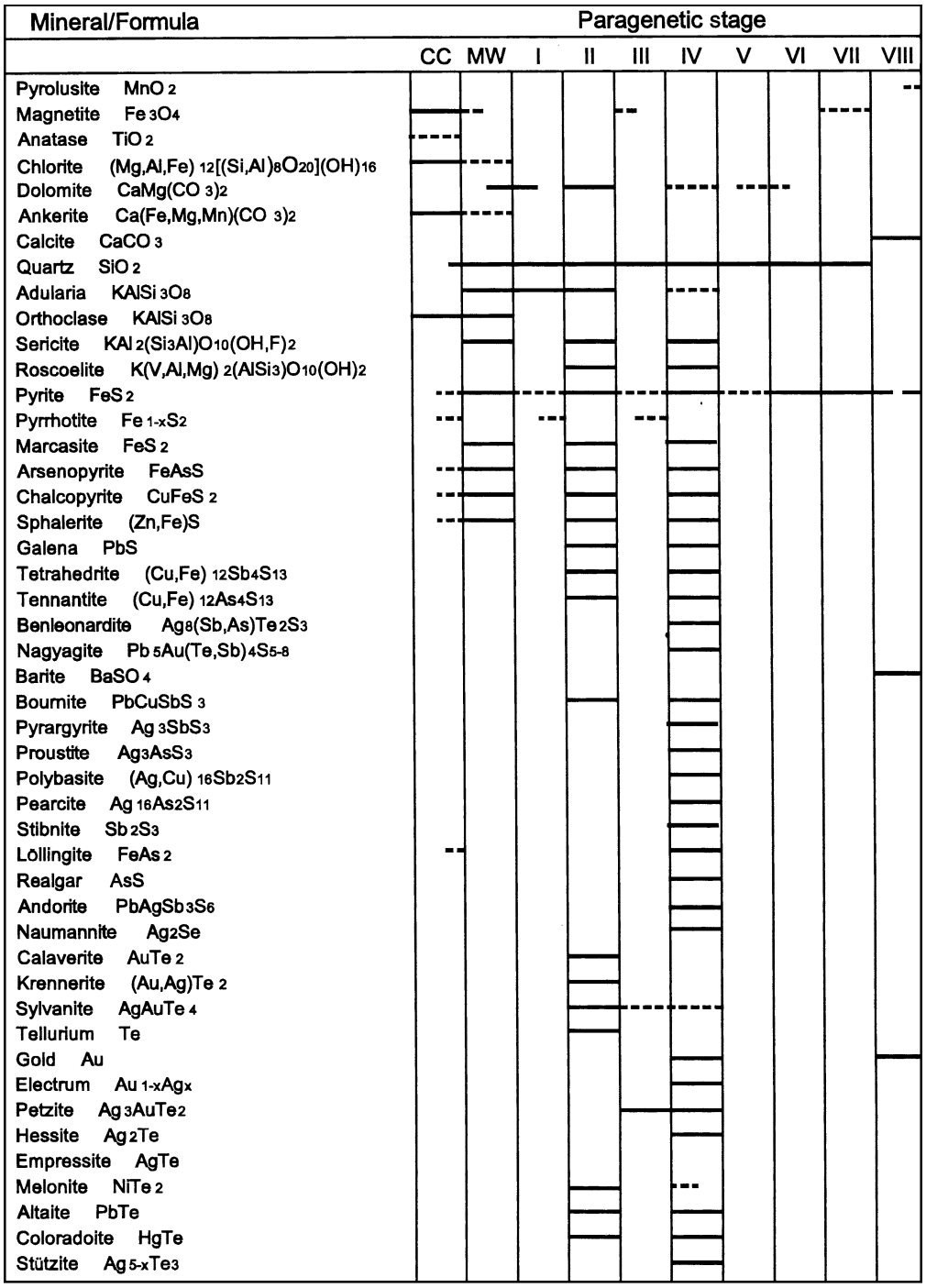

CC Chlorite–Carbonate rock; *MW* Mineralized wall rock

EDAX area mapping and back scattered imaging capabilities to evaluate the distribution of elements in individual grains.

Sample selection and paragenetic studies

One hundred and eighteen samples were collected from underground locations, drill core, and from *Begg's* (1996) research collection primarily from the Matanagata and Matanagata East Flatmakes and the R1 Zone. Most samples in the R1 zone were obtained from the Kava Flatmake, the UFZ lode, and the Crown Cross system (Figs. 2 and 3).

Slabs of veins (up to 15 cm wide) and surrounding alteration zones were collected from several locations in each of the three major areas studied. Multiple polished thin sections were subsequently made from these slabs to make sure that as much of the paragenetic sequence could be evaluated as possible at a given location. Within the crustified quartz–carbonate veins distinct stages of vein growth can be recognized. However, it should be stressed that only two to four stages were generally recognized in individual samples. The various sulfide or telluride stages are separated by barren quartz stages but, within a given stage, pyrite with inclusions of sulfides and tellurides can be overgrown by pyrite with inclusions of different sulfides and tellurides from a later stage. The pyrite stages were distinguished on the basis of concentric patterns formed when etched with 1:1 HCl-$KMnO_4$ and back-scattered images and X-ray element maps using the Hitachi SEM (see Fig. 6 of *Pals* et al., 2003). Reflected light, electron microprobe studies, and qualitative SEM analyses confirmed the identity of most of the minerals identified by *Ahmad* et al. (1987) in a given stage. The first seven stages are dominated by quartz and the eighth by calcite. Stages II and IV are the ore-bearing stages with stage II consisting predominantly of pyrite, sphalerite, chalcopyrite, and tetrahedrite-tennantite, as well as tellurium-bearing minerals (sylvanite ($AuAgTe_4$), calaverite ($AuTe_2$), krennerite ($(Au,Ag)Te_2$), native tellurium, altaite (PbTe), and coloradoite (HgTe). Stage IV contained essentially the same minerals as stage II

Fig. 4. Reflected light photomicrographs (a to g) and a SEM back-scattered image (h) **a** Stage II feathery pyrite. The lowest, central grain contains 5.67 wt.% As (sample 99EM-8a, Matanagata East flatmake; plane polarized light); **b** Stage II pyrite cube in compositionally zoned stage IV sphalerite (sample 99EM108, 2000N flatmake; cross polarized light); **c** Stage IV chalcopyrite, pyrite, sphalerite, tennantite, and tetrahedrite in quartz (Qtz) (sample 99EM62, Matanagata flatmake; plane polarized light); **d** Stage II krennerite and sylvanite (showing parasynthetic twins) overgrown by stage IV hessite in quartz (Qtz) (99EM94c; Prince William flatmake; cross polarized light); **e** Stage III petzite (Petz) and sylvanite (Sylv) in quartz (Qtz) (sample 99EM62, Matanagata flatmake; plane polarized light); **f** Stage III petzite (Petz) and sylvanite (Sylv) in quartz (Qtz) (sample 99EM12a, Matanagata flatmake; plane polarized light); **g** Stage IV petzite and coexisiting electrum in pyrite (sample 99EM14, Matanagata flatmake; plane polarized light); **h** SEM back-scattered image of stage IV benleonardite, tennantite, and pyrite in quartz (sample 99EM75 (Begg's sample VJ34558), Prince William flatmake)

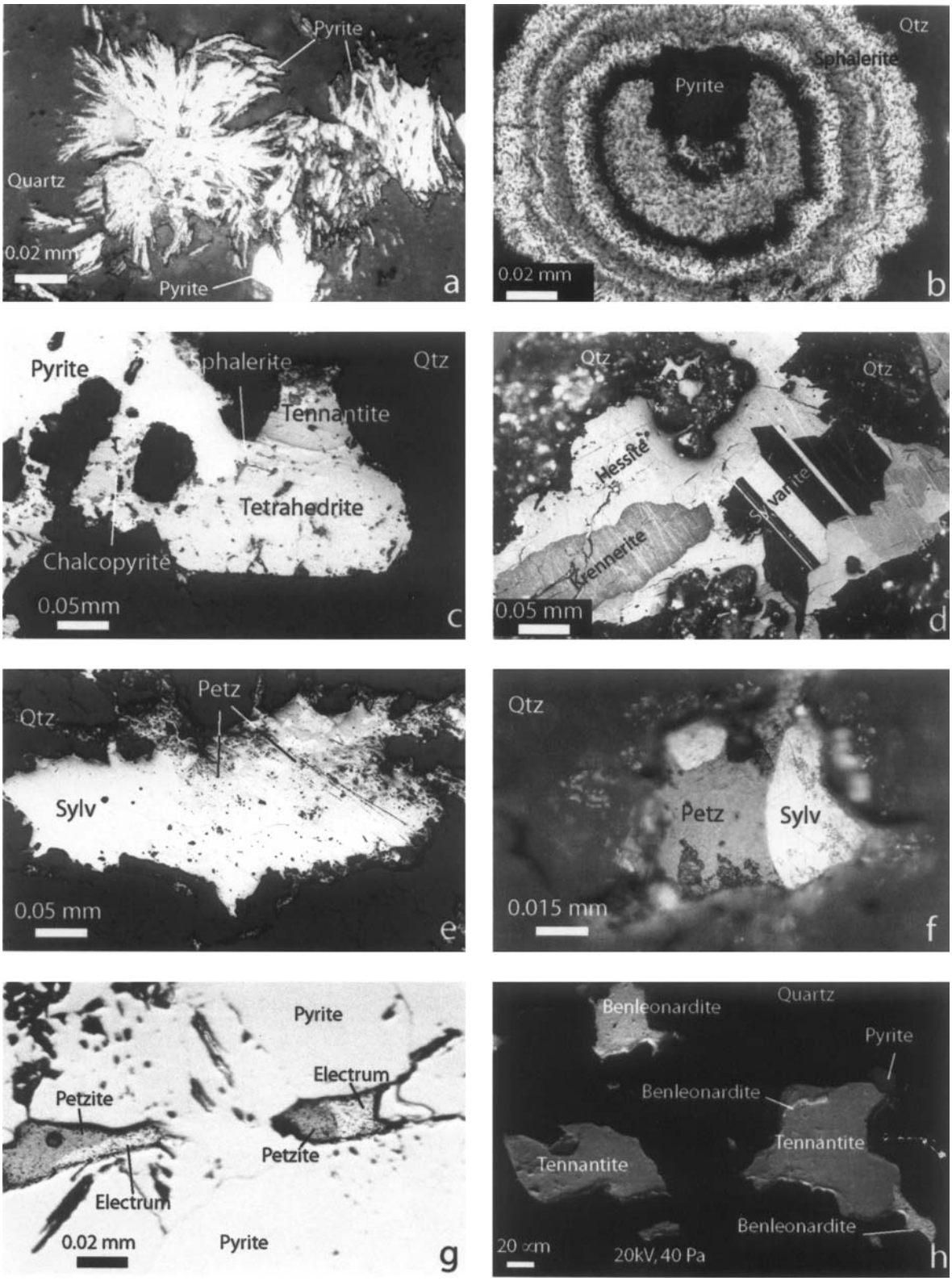
Pyrite
Quartz
0.02 mm
Pyrite
a
Qtz
Sphalerite
Pyrite
0.02 mm
b
Pyrite
Sphalerite
Qtz
Tennantite
Tetrahedrite
Chalcopyrite
0.05mm
c
Qtz
Qtz
Hessite
Krennerite
0.05 mm
d
Petz
Qtz
Sylv
0.05 mm
e
Qtz
Petz
Sylv
0.015 mm
f
Pyrite
Electrum
Petzite
Petzite
Electrum
0.02 mm
Pyrite
g
Benleonardite
Quartz
Pyrite
Benleonardite
Tennantite
Tennantite
Benleonardite
20 µm
20kV, 40 Pa
h

but the precious metal minerals consist of petzite (Ag_3AuTe_2), hessite (Ag_2Te), and native gold. In addition to the ore-bearing stages identified by *Ahmad* et al. (1987), it should be noted that stages III and VIII also contain precious metal minerals. Stage III contains rare sylvanite and petzite while stage VIII contains rare platelets of native gold up to 5 mm in length intergrown with or perched on calcite. Hydrothermal stages can be correlated from one flatmake to the other regardless of the structural setting and the proposed temporal relationship among flatmakes that were recognized by *Begg* (1996). We support the view of *Ahmad* et al. (1987) that there are eight major stages (I–VIII) of hydrothermal mineral deposition in the Emperor deposit and will use the vein-stage terminology of *Ahmad* et al. (1987) for the remainder of this paper. We have developed a modified paragenetic sequence of *Ahmad* et al. (1987) to incorporate three minerals, benleonardite ($Ag_8(Sb,As)Te_2S_3$), andorite ($PbAgSb_3S_6$), and naumannite (Ag_2Se), which we have identified for the first time at Emperor (Table 1), and pyrolusite, which was recently reported by *Lawrence* et al. (2001). Andorite occurs as lath-like blades up to 160 μm in length in quartz from Prince William flatmake.

Pyrite

Pyrite constitutes $>95\%$ of the total sulfide, sulfosalt, telluride, and native element content of the Emperor deposit and about 0.5 to 1% of the mined ore. It occurs in a variety of forms including individual feathery laths (3 to 20 μm in length) or aggregates of laths (up to 200 μm in length) (Fig. 4a), isolated grains or masses of inclusion-free, subhedral to euhedral pyritohedrons and cubes (20 μm to 2 mm in diameter), anhedral masses of grains, skeletal crystals, and brecciated grains. Marcasite formed as a replacement of earlier formed pyrite and pyrrhotite. In places, individual pyrite cubes occur in spectacular color-zoned sphalerite (Fig. 4b)

The intimate relationship between invisible gold and arsenian pyrite and arsenopyrite is known from several epithermal gold deposits worldwide (e.g., *Cook* and *Chryssoulis*, 1990; *Fleet* et al., 1993; *Simon* et al., 1999a, b). On the basis of bulk-compositional data on concentrates, *Stillwell* and *Edwards* (1946) first pointed out that ''invisible gold'' occurred in pyrite and arsenopyrite at Emperor but they did not recognize the pyrites were arsenian. However, *Jamieson* and *Ryan* (1993) analyzed pyrite in a quartz–pyrite–gold vein using combined micro particle induced X-ray emission and channeling contrast microscopy and found that Au occurs as minute Au-bearing minerals and as Au in solid solution in the structure of pyrite. Arsenian pyrite manifests itself as uniformly distributed grains, as arsenic-rich rims on preexisting grains, or as arsenic-rich cores. Each stage of pyrite growth can be correlated with a given hydrothermal stage in the paragenetic sequence. Details of the ''invisible gold'' and ''invisible tellurium'' content of arsenian pyrite in the Emperor deposit are given in *Pals* et al. (2003) and will only be summarized here. Scanning electron microscopy (SEM), electron probe microanalysis (EPMA), and secondary ion mass spectroscopy (SIMS) by *Pals* et al. (2003) show that pyrite from Emperor is among the most Au- (up to 11,057 ppm Au), Te- (up to 5,796 ppm Te), and As-rich (up to 16.60 wt.% As) yet reported. The highest invisible gold, arsenic, and tellurium contents occur in stages II and IV, which are the stages

Table 2. *Representative electron microprobe analyses of tetrahedrite group minerals and benleonardite*

	1	2	3	4	5	6	7	8	9	10
Cu	31.43	41.26	37.62	42.94	41.66	35.94	0.18	0.30	0.00	0.31
Ag	11.49	1.00	1.91	0.34	0.00	2.28	63.00	64.87	65.50	64.83
Fe	0.11	5.27	0.35	0.70	2.85	0.50	0.00	–	–	–
Zn	7.30	0.00	9.64	6.13	6.24	8.00	0.00	0.34	0.46	0.00
Sb	15.50	13.53	16.64	0.46	0.00	19.40	5.81	6.60	6.99	6.88
As	8.84	11.45	8.13	17.69	21.72	6.50	1.57	1.71	1.20	1.66
Bi	0.00	0.00	0.15	0.00	0.00	0.11	0.00	–	–	–
Te	0.00	0.00	0.41	3.86	0.00	0.00	19.99	19.24	18.78	19.98
S	26.00	26.61	26.49	28.18	28.28	26.27	8.22	8.47	8.27	8.38
	100.67	99.24	101.34	100.30	100.75	99.00	98.77	101.53	101.20	102.04
No of atoms	29	29	29	29	29	29	14	14	14	14
Cu	9.003	10.178	9.338	10.132	9.632	9.195	0.038	0.060	0.000	0.062
Ag	1.744	0.145	0.279	0.047	0.000	0.344	7.654	7.631	7.802	7.648
Fe	0.032	1.481	0.099	0.188	0.750	0.146	0.000	–	–	–
Zn	1.828	0.000	2.325	1.406	1.402	1.989	0.000	0.066	0.090	0.000
Sb	2.085	1.744	2.156	0.057	0.000	2.590	0.625	0.688	0.697	0.690
As	1.931	2.397	1.711	3.539	4.257	1.410	0.274	0.290	0.206	0.282
Bi	0.000	0.000	0.011	0.000	0.000	0.009	0.000	–	–	–
Te	0.000	0.000	0.051	0.454	0.000	0.000	2.045	1.913	1.891	1.993
S	13.277	13.011	13.030	13.177	12.959	13.317	3.364	3.352	3.314	3.326

1 Argentian tetrahedrite (99EM75); *2* Tennantite (99EM10A); *3* Tetrahedrite 99EM17A; *4* Tellurium bearing tennantite (99EM94B); *5* Tennantite (99EM94C); *6* Tetrahedrite (99EM1A); *7* Benleonardite (99EM75) – Emperor; *8–10* – Benleonardite (USY-1) – Um Samiuki, Egypt (*H.M. Helmy*, unpublished data)

that contain the highest proportion of gold-bearing tellurides. *Pals* et al. (2003) estimated that the proportion of gold as ''invisible gold'' at Emperor ranges from 47 to 90%.

Tetrahedrite group minerals

Apart from pyrite, tetrahedrite group minerals are the most common minerals intergrown with precious metal tellurides. Seventy-three electron microprobe analyses of tetrahedrite group minerals (or fahlores) exhibit a wide range of compositions from tetrahedrite to tennantite ($Sb/(Sb + As) = 0.00$ to 0.87) with Zn- and Fe-rich varieties of both end-members ($Zn/(Zn + Fe) = 0.01$ to 0.99) (Table 2; Fig. 5). Of these analyses, 50 are of tennantite and 23 are of tetrahedrite. Note that *Ahmad* et al. (1987) reported tetrahedrite, rather than tennantite, as the fahlore at Emperor. In places, tetrahedrite and tennantite coexist (Fig. 4c) but isolated tetrahedrite crystals sitting on quartz (up to 7 mm in length) are also known (*Lawrence* et al., 2001). Silver-rich euhedral tennantite (6.01 wt.% Ag) occurs in one sample from the Prince William flatmake where it is intergrown with benleonardite and spatially associated with pyrargyrite, chalcopyrite, sylvanite, krennerite, and hessite. Similarly, *Knights* (2000) in a recent mineralogical study of roaster feed concentrate from Emperor proposed, on the basis of optical studies, that a ''probable silver tetrahedrite (freibergite?)'' was encountered. However, our studies suggest Ag-rich tetrahedrite group minerals at Emperor do not contain sufficient Ag to be termed ''freibergite.'' Moreover, our data suggest the Ag-rich tetrahedrite group mineral identified by *Knights* (2000) was likely to be Ag-bearing tennantite rather than Ag-rich tetrahedrite.

Hackbarth and *Petersen* (1984), *Sack* (1992) and *Sack* et al. (2002) proposed that the composition of tetrahedrite–tennantite can be used to determine such things as temperature of the ore fluid and fluid flow directions in a given deposit

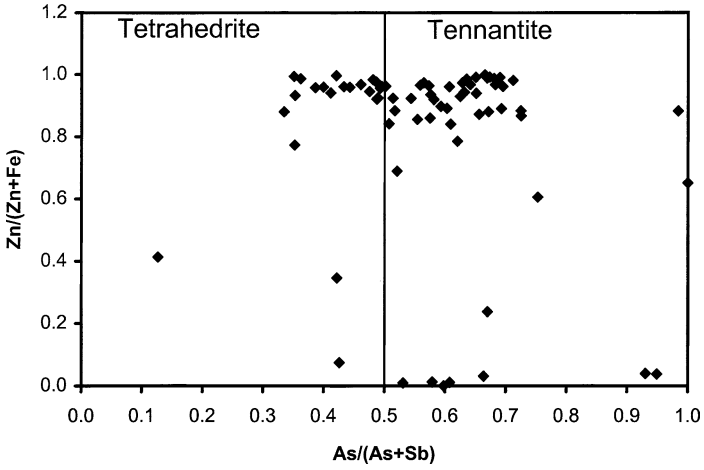

Fig. 5. Chemical variation of tetrahedrite–tennantite fahlores from the Emperor deposit as a function of $Zn/(Zn + Fe)$ versus $As/(As + Sb)$

or ore district. These parameters are dependent upon the coupled substitution between Fe and Zn, Cu and Ag, and As and Sb as a result of exchanges of these elements between tetrahedrite–tennantite and coexisting sulfides–sulfosalts. Unfortunately, the sulfide/sulfosalt assemblage at Emperor does not allow these parameters to be derived since Zn-rich sulfides such as sphalerite (Fig. 4c), and Ag-rich sulfosalts (proustite, pearcite, polybasite, and pyrargyrite) rarely coexist with tennantite or tetrahedrite. However, it should be noted that the majority of tetrahedrite–tennantite fahlores at Emperor exhibit $Zn/(Zn + Fe)$ and $As/(As + Sb)$ ratios of 0.80 to 0.99 and 0.32 to 0.71 (Fig. 5), respectively, suggesting rather uniform ore fluid compositions for stages II and IV.

Tellurides

Introduction

Of the ten tellurium-bearing minerals, sylvanite, calaverite, krennerite, petzite, hessite, empressite, coloradoite, altaite, melonite, and native tellurium, that were reported previously in the Emperor deposit (*Stillwell*, 1949; *Ahmad* et al., 1987), only melonite and altaite were not identified in the present study. However, the rare sulfotelluride, benleonardite, is recognized for the first time. Although most of these Te-bearing minerals occur as inclusions in pyrite and tetrahedrite group minerals, the most spectacular tellurium-bearing minerals occur as isolated crystals or clusters of crystals (e.g. sylvanite, native tellurium, and krennerite), up to several cm in length, intergrown with or perched on quartz crystals (*Lawrence* et al., 2001). Representative analyses of some of the Te-bearing minerals are given in Table 3 whereas a complete list of compositions of all tellurides can be found in *Pals* (2002). Brief descriptions of individual tellurides observed in the present study are given below.

Sylvanite

Sylvanite $AgAuTe_4$, the most abundant telluride in the Emperor deposit (Fig. 2) possesses a variety of grain sizes and shapes and occurs in several different assemblages (Fig. 4d, e, and f). It shows no uniform distribution within flatmakes (e.g. Prince William, Fig. 2) but it is most abundant where flatmakes intersect steep structures, faults, or shatters zones (e.g. Matanagata East, Kava, and 2000N flatmakes, Fig. 2).

Laths of sylvanite spatially associated with acicular grains of krennerite form in the Prince William flatmake whereas anhedral grains of sylvanite from the Matanagata and Matanagata East flatmakes are intergrown with native tellurium. Sylvanite is also commonly intergrown with tetrahedrite, tennantite, calaverite, stützite, hessite (Figs. 4e and f), pyrite, chalcopyrite, sphalerite, and galena.

Krennerite

After sylvanite, krennerite $(Au,Ag)Te_2$ is the next most common precious metal telluride in the Emperor deposit. Krennerite shows no uniform distribution within a given flatmake but, like sylvanite and calaverite, it is more common in and adjacent

Table 3. *Composition of tellurium-bearing minerals from the Emperor deposit*

	1	2	3	4	5	6	7	8	9
Au	0.00	27.04	31.76	0.05	23.57	35.83	0.64	0.20	43.46
Ag	0.00	11.25	6.52	57.38	41.82	4.90	62.55	62.32	0.49
Bi	0.05	0.06	0.00	0.00	0.11	0.29	0.00	0.00	0.11
Te	99.87	61.15	60.25	41.51	33.29	58.42	37.12	27.00	57.43
Se	0.00	0.00	0.00	0.00	0.00	0.00	0.00	8.58	0.00
S	0.00	0.04	0.00	0.00	0.13	0.00	0.00	0.69	0.00
Total	99.92	99.54	98.53	98.94	98.92	99.44	100.31	98.77	101.49
No. of atoms	1	6	6	8	6	3	3	3	3
Au	0.000	1.143	1.392	0.003	0.929	0.795	0.011	0.003	0.977
Ag	0.000	0.868	0.522	4.952	3.010	0.198	1.990	1.883	0.020
Bi	0.001	0.000	0.000	0.000	0.004	0.006	0.000	0.000	0.002
Te	0.999	3.989	4.077	3.028	2.026	2.001	0.999	0.691	1.991
Se	0.000	0.000	0.000	0.000	0.000	0.000	0.000	0.354	0.000
S	0.000	0.002	0.000	0.017	0.031	0.000	0.000	0.069	0.000

1 Native tellurium (99EM110A); *2* Sylvanite (00EM67); *3* Sylvanite (99EM62); *4* Stützite (00EM67); *5* Petzite (99EM94C); *6* Krennerite (00EM112); *7* Hessite (99EM75); *8* Selenian hessite (99EM75); *9* Calaverite (99EM72B); Data in the table are individual point analyses; detection limits are <0.1 wt.%

to the intersection of flatmakes with vertical structures and shatters zones (Fig. 3). It occurs in the North Dipper, Prince, Matanagata, and Prince William flatmakes, and the Sultan Shatter and R1 zones, as anhedral to subhedral tabular grains usually less than 0.5 mm in length (Fig. 4d).

Calaverite

Calaverite $AuTe_2$ was only identified herein in three samples from the Matanagata East flatmake. However, *Begg* (1996) previously identified it in samples from the Crown deposit, the Koreore Hill and Emperor Shatter zones, and the Prince and Prince William flatmakes. In the Matanagata East flatmake, calaverite occurs as inclusions or masses in arsenian pyrite or as lath-like or euhedral grains intergrown with sylvanite or native tellurium.

Native tellurium

Native tellurium occurs as intergrowths with sylvanite, calaverite, krennerite, hessite, chalcopyrite, and tetrahedrite. It is most common in R1 lodes where it coexists mainly with sylvanite or with sylvanite and calaverite. The assemblage native tellurium–calaverite was observed in the Matanagata East flatmake whereas native tellurium–hessite occurs as inclusions in pyrite.

Hessite

Hessite Ag_2Te is less abundant than native tellurium and gold- and gold–silver tellurides. It was observed as inclusions in tetrahedrite, as an intergrowth with

petzite and electrum in samples from the Matanagata flatmake, as overgrowths of stage II krennerite and sylvanite (Fig. 4d), and as inclusions or intergrowths with silver-rich tennantite and naumannite in pyrargyrite (Ag_3SbS_3) in the Prince William flatmake, and possibly as intergrowths with benleonardite. Based on three electron microprobe analyses, hessite with between 1.3 and 8.6 wt. Se was recorded and suggests the possibility of an incomplete solid solution between hessite and naumannite (Table 3). Naumannite, although only up to 5 μm in size, was identified by partial electron microprobe analyses and elemental mapping as inclusions in contact with hessite and silver-rich tetrahedrite in pyrargyrite in the Prince William flatmake.

Petzite

In stage III in the Matanagata flatmake, rare subhedral to anhedral petzite (15 μm to approximately 1 mm) occurs as intergrowths (Fig. 4e) or as separate coexisting grains with sylvanite (Fig. 4f), and in otherwise barren cockscomb quartz. The intergrowth between petzite Ag_3AuTe_2 and sylvanite may be a breakdown product of *Cabri's* (1965) gamma-phase that formed below 120 °C (Fig. 4e). Stage IV petzite and electrum intergrowths are present as inclusions in pyrite in the Matanagata flatmake (Fig. 4g). In addition, stage IV petzite is also intergrown with hessite and stützite or hessite and electrum.

Coloradoite

Coloradoite (HgTe) was first identified in the Emperor deposit by *Stillwell* (1949) coexisting with an unidentified telluride but was identified herein as intergrowths (2 to 5 μm in length) with krennerite, along grain boundaries with pyrite, and coexisting with chalcopyrite, tennantite, and sphalerite in the Matanagata flatmake.

Benleonardite

Benleonardite $Ag_8(Sb,As)Te_2S_3$ is present in sample 99EM75 (Begg's sample VJ34558) from the Prince William flatmake, where it occurs as isolated inclusions up to 60 μm in length in quartz and as inclusions in tennantite (Fig. 4h). *Markham* (1960, p. 1470) reported "gold and hessite are intimately associated with an unknown blue-gray telluride showing weak pleochroism and moderate anisotropism." It is likely that this blue-gray telluride was benleonardite since it possesses the same optical properties as those described for benleonardite elsewhere in the literature (e.g., *Stanley* et al., 1986; *Spry* and *Thieben*, 1996).

Benleonardite was first identified by *Stanley* et al. (1986) and *Criddle* et al. (1989) from the Bambolla silver telluride deposit but reports of benleonardite-like minerals in the literature were given by *Aksenov* et al. (1969), *Karup-Møller* and *Pauly* (1979), and *Zhang* and *Spry* (1994b) from the Zyranov gold deposit (Russia), Ivigtut cryolite deposit (Greenland), and the Gies gold–silver telluride deposits (Montana), respectively. Benleonardite has since been reported in the epithermal Mayflower gold–silver telluride deposit, Montana (*Spry* and *Thieben*, 1996), the Um Samiuki Zn–Pb–Cu–Ag volcanogenic massive sulfide deposit, Egypt (*Helmy*

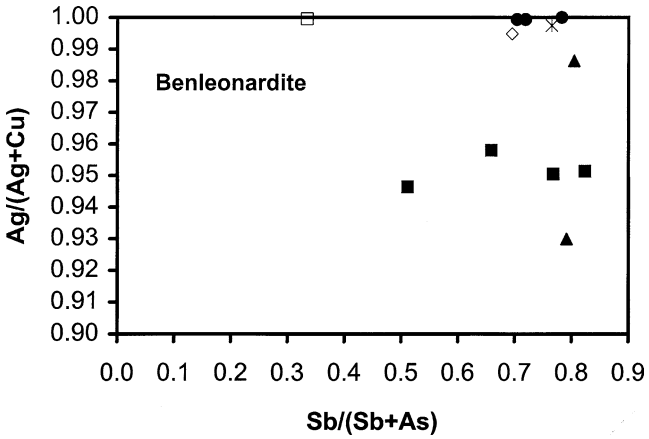

Fig. 6. Chemical variation of benleonardite from worldwide locations as a function of $Ag/(Ag + Cu)$ versus $Sb/(Sb + As)$. Compositions of benleonardite are from Bambolla, Mexico (cross; *Stanley* et al., 1986), Emperor, Fiji (diamond; this study), Gies, Montana, U.S.A. (filled squares; *Spry* and *Thieben*, 1996), Mayflower, Montana, U.S.A. (triangle; *Spry* and *Thieben*, 1996), Rotgülden, Austria (open square; *Horne* et al., 1997), and Um Samiuki, Egypt (circles; this study)

et al., 1999), and in black smoker chimney fragments from the Yaman Kasy massive sulfide deposit, southern Urals (*Herrington* et al., 1998).

Based on all available benleonardite compositions reported in the literature (*Spry* and *Thieben*, 1996), that from Emperor, and three new unpublished data from the Um Samiuki deposit (Table 2), it would appear that the amount of As that can substitute for Sb is up to 30% and that Ag can substitute for up to nearly 10% of the Cu sites (Fig. 6). The compositions of benleonardite-like minerals from the Zyranov gold (*Aksenov* et al., 1969) and Ivigtut cryolite deposits (*Karup-Møller* and *Pauly*, 1979) were not included in Fig. 6 because As was not analyzed. Benleonardite from the Emperor deposit exhibits similar $Ag/(Ag + Cu)$ and $Sb/(Sb + As)$ ratios to those from the Bambolla and Um Samiuki deposits. Like those from other locations, benleonardite from Emperor exhibits a slight deficiency in $Ag + Cu$ (i.e., < 8 atoms per formua unit) coupled with a slight excess in S (i.e., 3 to 4 atoms per formula unit). Its composition, along with those from Um Samiuki, reinforces the suggestion by *Spry* and *Thieben* (1996) that the formula proposed by *Stanley* et al. (1986) needs to be modified.

Discussion

Previous mineralogical studies of telluride-bearing mineralization focused on flatmakes, steep structures, and shatter zones in the central and western parts of the Emperor deposit (e.g., *Stillwell*, 1949; *Forsythe*, 1971; *Ahmad* et al., 1987; *Kwak*, 1990). By comparison, the Matanagata and Matanagata East flatmakes and R1 zone have received only limited attention (*Nand* and *Reid*, 1998). Twenty-two samples from the Matanagata flatmake and three samples from the R1 zone were examined by *Begg* (1996), but sylvanite and petzite were identified in only one

sample from each of these ore zones. No studies were conducted on samples from the Matanagata East flatmake. *Poliquin* (1996) identified sylvanite in only one sample from R1.

The current study shows the presence of nine tellurium-bearing minerals in thirteen assemblages (sylvanite–calaverite, sylvanite–krennerite, sylvanite–native tellurium, sylvanite–stützite, sylvanite–hessite, sylvanite–petzite, calaverite–native tellurium, krennerite–native tellurium, hessite–native tellurium, hessite–petzite, hessite–petzite–electrum, petzite–stützite–hessite, coloradoite–krennerite). Twelve of these assemblages exclusively involve minerals in the system Au–Ag–Te. The precious metal assemblages, along with all compositions of tellurides and native tellurium analyzed here reveal, on a ternary plot in terms of Au, Ag, and Te (Fig. 7), that precious metal assemblages evolve from Te- and Au-rich assemblages (stage II) to Ag-rich and intermediate Te-bearing assemblages (stage III), and finally to Te-poor assemblages (stage V).

Experimental studies of *Cabri* (1965) show that sylvanite contains 6.7 to 13.2 wt.% Ag, with the highest Ag content being that of ''theoretical'' sylvanite. According to *Stumpfl* (1970), sylvanite at Emperor is unusual in composition because it contains the whole range of Ag contents from ''6–12 wt.% Ag.'' Four analyses of unlocated samples of sylvanite by *Lawrence* et al. (2001) range from 11.25 to 13.23 wt.% Ag. However, seventy-four additional electron microprobe

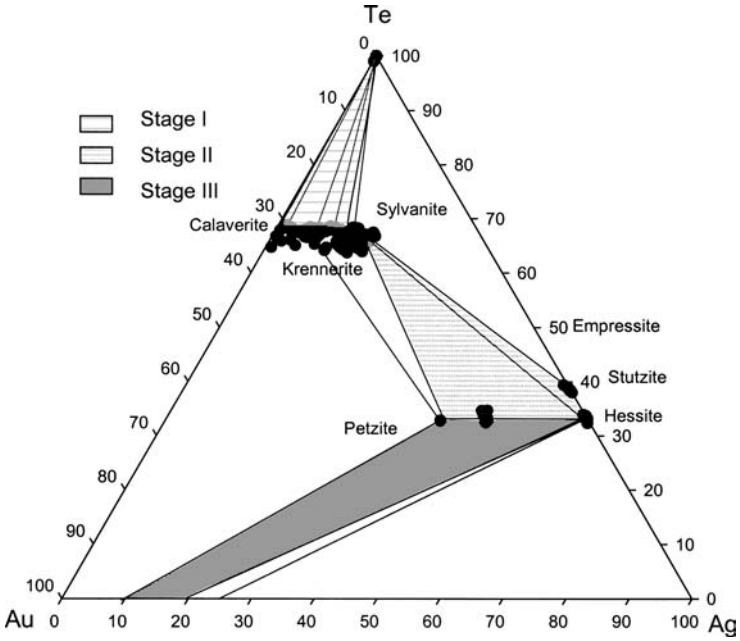

Fig. 7. Ternary diagram of the system Au, Ag, and Te in atomic proportions for minerals analyzed in the present study from the Emperor deposit. All data are listed in *Pals* (2002). Solid lines indicate representative compositions of coexisting phases. Stage II assemblages are Te- and Au-rich whereas stage III assemblages are Ag-rich. Stage IV precious metal assemblages are Te-poor and contain Ag-rich tellurides plus native gold/electrum. Note the continuum of compositions among calaverite, krennerite, and sylvanite

analyses obtained herein reveal that sylvanite ranges in composition from 6.28 to 13.45 wt.% Ag. As to be expected from phase relations in the system Au–Ag–Te, sylvanite in equilibrium with hessite or stützite at Emperor is Ag-rich whereas that in contact with calaverite or krennerite is Ag-poor. As with sylvanite, krennerite is usually depleted in Ag relative to krennerite found in other epithermal gold–silver telluride deposits. *Cabri* (1965) noted natural and synthetic krennerite contains approximately 5 wt.% Ag and 3.3 to 6.2 wt.% Ag, respectively. Krennerite at Emperor ranges in composition from 3.0 to 5.9 wt.% Ag (n = 33). Silver-poor krennerite occurs in grains in close spatial proximity to or intergrown with arsenian pyrite in the Dolphin orebody. Experiments by *Cabri* (1965) also show that calaverite contains up to 2.9 wt.% Ag. At Emperor, calaverite compositions range from 0.5 to 3.1 wt.% Ag (n = 14).

Using an average temperature of 250 °C for stage II mineralization, based on the fluid inclusion studies of *Ahmad* et al. (1987), *Kwak* (1990), *Begg* (1996) and *Poliquin* (1996), the stability of tellurides and sulfides, and the composition of sphalerite coexisting with pyrite and tellurides, log fS_2 and log fTe_2 conditions for stage II were restricted to −12.7 to −10.1 and −9.4 to −7.8, respectively (Fig. 8). Thermodynamic data for sulfides and tellurides used for calculating Fig. 8 were derived from *Mills* (1974), *Barton* and *Skinner* (1979), and *Afifi* et al. (1988).

The present study, along with earlier studies (*Stillwell* and *Edwards*, 1946; *Stillwell*, 1949; *Markham*, 1960; *Forsythe*, 1967, 1971; *Stumpfl*, 1970; *Ahmad* et al., 1987; *Kwak*, 1990; *Begg*, 1996), show that the spatial distribution of individual tellurides changes dramatically within a given flatmake, steep structure, or shatter zone. Although more concerned with the vertical variation in Ag:Au and (Au + Ag):Te ratios, *Forsythe* (1967, 1971) showed, in a general sense, the more

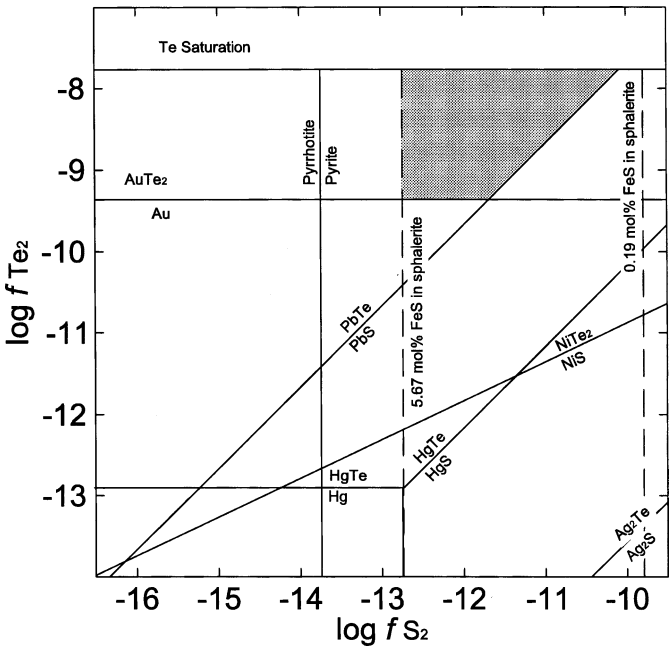

Fig. 8. Log fTe_2 versus logfS_2 diagram calculated at 250 °C. Shaded area indicates mineral stabilities calculated from sphalerite and observed mineral assemblages. Sources of data are listed in text

gold-rich tellurides (krennerite, sylvanite and calaverite) occur near the upper part of the Crown-Crescent lode (i.e. above the 13 level) whereas the silver-rich tellurides, petzite and hessite, along with native gold extend down to the 16 level. With regards to the system Au–Ag–Te, it appears the assemblages calaverite–krennerite–sylvanite and sylvanite–krennerite, which occur toward the left-hand side of Fig. 7, are stable toward the top of the Crown-Crescent lode but are replaced by the stable ternary assemblage petzite–hessite-native gold (central-bottom of Fig. 7) with depth. However, what is unclear from *Forsythe's* (1967, 1971) studies is whether these minerals are all from the same hydrothermal stage because calaverite–sylvanite–krennerite is more common in stage II whereas the assemblage petzite–hessite-native gold is more abundant in stage IV. Despite this uncertainty, it is critical to realize a high sampling density is required to establish zonation patterns. Note *Forsythe* (1967, 1971) used 76 samples in his studies of the Crown-Crescent lode.

To evaluate the spatial distribution of tellurides at Emperor, it is essential that the temporal relationship among tellurides be determined first and that the conflict regarding the paragenetic sequence, which arose as a result of the studies of *Ahmad* et al. (1987) and *Begg* (1996), be resolved. Paragenetic studies conducted as part of the present investigation support the views of *Ahmad* et al. (1987). Samples studied herein consistently show that Ag-rich tellurides, petzite and hessite, along with native gold, formed later than Au-rich tellurides, calaverite, krennerite, and sylvanite. Although this observation alone does not rule out *Begg's* (1996) interpretation that there were at least 40 ore-forming cycles associated with the formation of the Emperor deposit, such a high number of cycles and stages of telluride formation is inconsistent with the observations here and with telluride parageneses in other gold telluride deposits. Where Au-rich and Ag-rich tellurides are found in the same deposit, Au-rich tellurides most commonly formed prior to Ag-rich tellurides (see for example, *Zhang* and *Spry*, 1994a, b; *Spry* et al., 1997, *Spry* and *Thieben*, 2000). The Emperor deposit does not appear to be an exception to this observation. A very unusual set of physical and chemical conditions would be required by *Begg* (1996), to form the multiple, but similar, generations of telluride stages among the various flatmakes and ore-bearing steep structures, especially since he considered that each of these auriferous zones formed at different times during the evolution of the Emperor deposit.

Given the optical similarity between krennerite and sylvanite and the fact sylvanite and krennerite at Emperor commonly exhibit compositions close to those that distinguish Ag-poor sylvanite from Au-rich krennerite and Au-rich calaverite from Ag-poor krennerite, raises the question of the veracity of the identification of calaverite, krennerite, and sylvanite at Emperor by such methods. Therefore, caution must be made when incorporating mineralogical data of Au-rich tellurides from other studies if they are based on optical data only. Note that coarse sylvanite is easily identified in reflected light because it generally exhibits multiple twins. However, fine-grained sylvanite can easily be confused with krennerite if multiple twins are absent.

Apart from *Forsythe's* (1967, 1971) studies of the Crown-Crescent lode, no other study has evaluated enough samples from a given flatmake, shatter zone, or steep structure to allow any meaningful discussion of the spatial distribution

of precious metal tellurides to be made. *Begg* (1996) obtained 67 samples from several flatmakes, steep structures, and shatter zones, of which, 46 were from the Prince William flatmake. Begg's samples were well located and can, in principle, be used to ascertain the distribution of tellurides in this flatmake. His studies showed sylvanite, krennerite, and petzite are the most abundant tellurides in the Prince William flatmake followed by calaverite. Despite the limited number of samples from each orebody, studies of sylvanite, krennerite, and calaverite in the Matanagata East, Matanagata, 2000N, Prince William, and Kava flatmakes and the UFZ lode in the present study (Figs. 2 and 3) show that there is no systematic distribution of these three Au-rich tellurides within flatmakes. Instead, the abundance of tellurides increases where the flatmake intersects a steep structure or shatter zone or even where it comes in contact with a crosscutting andesite dike.

A clear genetic relationship between porphyry copper style mineralization and epithermal gold veins has been established and a magmatic origin has been proposed for the Emperor deposit (e.g., *Ahmad* et al., 1987; *Eaton* and *Setterfield*, 1993; *Begg*, 1996). The source of the ore-forming components for the epithermal gold mineralization remains speculative. However, the presence of krennerite, calaverite, colusite ($Cu_3(As,Sn,V)S_4$), and nekrasovite ($Cu_{26}V_2Sn_6S_{32}$) in ore from the Nasivi 3 porphyry copper deposit (*Eaton* and *Setterfield*, 1993) clearly indicates that Au, Te, V, were present in the porphyry system and in hydrothermal systems associated with the formation of the Tavua caldera. The same elements are common in the epithermal Emperor ores as evidenced by the presence of precious metal tellurides, roscoelite (i.e. V-rich), and chalcopyrite. Therefore, it is likely that pre-caldera monzonites were the source of the ore-forming components (*Eaton* and *Setterfield*, 1993). In this context, it is important to note that monzonite intrusions have been considered to be the source of ore-forming metals in epithermal gold telluride deposits elsewhere (e.g., Gies, Montana, *Zhang* and *Spry*, 1994b) including the nearby Tuvatu porphyry copper-epithermal gold telluride system, located 35 km southwest of the Emperor deposit, which is spatially and genetically related to the 4.5 Ma Navilawa Monzonite (*Scherbarth* and *Spry*, 2000).

Conclusions

1. Paragenetic and mineralogical studies show that nine tellurium-bearing minerals form in the eastern lodes (Matanagata, Matanagata East, and R1) in three (II, III, and IV) of the eight hydrothermal stages in the paragenetic sequence. The three most common gold-bearing tellurides are, in decreasing order, sylvanite, krennerite, and calaverite. Ag-rich tellurides, petzite and hessite, and native gold, formed later than the Au-rich tellurides.
2. Stage II tellurides formed at approximately 250 °C at $\log fS_2$ and $\log fTe_2$ of -12.7 to -9.8 and -9.4 to -7.8, respectively.
3. The nature and relative abundance of tellurides in the eastern orebodies, Matanagata, Matanagata East and R1, are the same as those reported previously for the central and western orebodies.
4. The spatial distribution of tellurides in the orebodies appears to be most abundant where flatmakes intersect steep structures, shatter zones, and andesite dikes. Individual tellurides show a patchy distribution within a given flatmake.

5. The source of most of the ore-forming metals, including Au, Ag, Te, Cu, V, and S, is likely to be pre-caldera monzonites spatially related to the gold system.

Acknowledgements

We thank Emperor Gold Mining Company Limited for financially supporting this project and company geologists, *T. Woodward, A. Czerw, P. Olubas, A. Nand*, and *D. Reid* for discussing various aspects of the geology and for guidance during underground and core shed visits. *PGS* appreciated discussions with *G. Begg* concerning his vast knowledge of the Emperor deposit and for providing us with a copy of his Ph.D. thesis. *A. Kracher* is thanked for his assistance with microprobe analyses. *H. Helmy* is gratefully acknowledged for providing unpublished electron microprobe compositions of benleonardite from the Um Samiuki deposit. The authors thank the editor *E. Stumpfl* and reviewers *C. Ciobanu* and *W. Paar* for their very helpful and constructive comments on the manuscript.

References

Afifi AM, Kelly WC, Essene EJ (1988) Phase relations among tellurides, sulfides, and oxides. I. Thermochemical data and calculated equilibria. Econ Geol 83: 377–394

Ahmad M, Solomon M, Walsh JL (1987) Mineralogical and geochemical studies of the Emperor gold telluride deposit, Fiji. Econ Geol 82: 345–370

Aksenov VS, Gavrilina KS, Litvinovich AN, Bespaev KHA, Pronin AP, Kosyak EA, Slyasarev AP (1969) Occurrence of new minerals of silver and tellurium in ores of the Zyranov deposits in the Altai (in Russian). Isvest Akad Nauk Kazakh SSR Ser Geol 3: 74–78

Alderton DHM, Fallick AE (2000) The nature and genesis of gold–silver–tellurium mineralization in the Metaliferi Mountains of western Romania. Econ Geol 95: 495–516

Barton PB Jr, Skinner BJ (1979) Sulfide mineral stabilities. In: *Barnes HL* (ed) Geochemistry of hydrothermal ore deposits. Wiley Interscience, New York, pp 278–403

Begg G (1996) The structure and mineralisation history of the Emperor gold deposit, Fiji. Thesis, Monash University

Begg G, Gray DR (2002) Arc dynamics and tectonic history of Fiji based on stress and kinematic analysis of dikes and faults of the Tavua Volcano, Viti Levu Island, Fiji. Tectonics 21: 1–14

Cabri LJ (1965) Phase relations in the Au–Ag–Te system and their mineralogical significance. Econ Geol 60: 1569–1606

Colley H, Flint DJ (1995) Metallic mineral deposits of Fiji. Fiji Mineral Res Dept Mem 4, 191 pp

Cook NJ, Chryssoulis SL (1990) Concentrations of invisible gold in common sulfides. Can Mineral 70: 591–594

Criddle AJ, Chisholm AE, Stanley CJ (1989) Cervelleite, Ag_4TeS, a new mineral from the Bambolla mine, Mexico, and a description of a photo-chemical reaction involving cervelleite, acanthite and hessite. Eur J Mineral 3: 371–380

Donovan JJ, *Rivers ML*, *Armstrong JT* (1992) PRSUPR: Automation and analysis software for wavelength dispersive electron-beam microanalysis on a PC. Am Mineral 77: 444–445

Eaton PC, Setterfield TN (1993) The relationship between epithermal and porphyry systems within the Tavua Caldera, Fiji. Econ Geol 88: 1053–1083

Fleet ME, Chryssoulis SL, MacLean PJ, Davidson R, Weisner CG (1993) Arsenian pyrite from gold deposits: Au and As distribution investigated by SIMS and EMP, and color staining and surface oxidation by XPS and LIMS. Can Mineral 31: 1–17

Forsythe DL (1967) Ore mineral distribution in the Crown-Crescent lode. Emperor gold mine, Fiji. Thesis, University of Melbourne

Forsythe DL (1971) Vertical zoning of gold–silver tellurides in the Emperor gold mine, Fiji. Proc Austral Inst Min Metall 240: 25–31

Gill JB, McDougall I (1973) Biostratigraphic and geological significance of Miocene-Pliocene volcanism in Fiji. Nature 241: 176–180

Gill JB, Whelan P (1989) Postsubduction ocean island alkali basalts in Fiji. J Geophys Res 94: 4579–4588

Hackbarth CJ, Petersen U (1984) A fractional crystallization model for the deposition of argentinian tetrahedrite. Econ Geol 79: 448–460

Helmy HM, Kamel OA, El Mahallawi MM (1999) Silver and silver-bearing minerals from the Precambrian volcanogenic massive sulfide deposit, Um Samiuki, Eastern Desert, Egypt. In: *Stanley* et al. (eds) Mineral deposits: processes to processing. Balkema, Rotterdam, pp 163–166

Herrington RJ, Maslennikov VV, Stanley CJ, Buslaev F (1998) Tellurium-bearing phases in black smoker chimney fragments from the Silurian Yaman Kasy massive sulphide orebody, southern Urals, Russia. 17th General Meeting International Mineralogical Association, Toronto, Abst Prog, A119 (Abstract)

Horne J, Neubauer F, Paar WH, Hansmann W, Koeppel V, Robl K (1997) Structure, mineralogy, and Pb isotopic composition of the As–Au–Ag deposit Rotgülden, Eastern Alps (Austria): significance for formation of epigenetic ore deposits within metamorphic domes. Mineral Deposita 32: 555–568

Jamieson DN, Ryan CG (1993) Microprobe channeling analysis of pyrite crystals. Instrumentation Methods Phys Res B77: 415–421

Karup-Møller S, Pauly S (1979) Galena and associated ore minerals from the cryolite at Ivigtut, S. Greenland. Meddelels Grønland Geosci 2: 1–25

Knights J (2000) Mineragraphy of Emperor gold roaster feed concentrate. Report to Emperor Gold Mining Co Ltd, 7 pp

Kwak TAP (1990) Geochemical and temperature controls on ore mineralization in the Emperor gold mine, Vatukoula, Fiji. J Geochem Expl 36: 297–337

Lawrence LJ, Sharpe JI, Williams PA (2001) Minerals of the Vatukoula gold mines, Fiji. Austr J Mineral 7: 63–72

Markham NL (1960) Synthetic and natural phases in the system Au–Ag–Te. Econ Geol 55: 1148–1178

Mills KC (1974) Thermodynamic data for inorganic sulfides, selenides, and tellurides. Butterworths, London

Nand AS, Reid DT (1998) Discovery and delineation of new orebodies at Vatukoula. Pacific Exploration Technology (PET 98) Conf Nadi, Fiji, September 23rd–25th, 1998 (Abstract)

Olubas P (1998) Geology of the Tavua Caldera. Field Excursion Guide, Emperor Gold Mining Co. Ltd, 5 pp

Pals DW (2002) Mineralogical studies of the Matanagata, Matanagata East, and R1 ore zones at the Emperor gold mine, Fiji. Thesis, Iowa State University

Pals DW, Spry PG, Chryssoulis S (2003) Invisible gold and tellurium in arsenic-rich pyrite from the Emperor gold deposit, Fiji: implications for gold distribution and deposition. Econ Geol 98: 479–493

Poliquin MJ (1996) Geological, geochemical and fluid inclusion studies of the R1 Zone, Emperor gold mine, Fiji. Thesis, University of Auckland

Rodda P (1993) Geology of Fiji. In: *Stevenson AJ, Herzer RH, Balance PF* (eds) Contributions to the marine and on-land geology and resource assessment of the Tonga-Lau-Fiji region. South Pacific Tech Bull No. 8

Rogers NW, Setterfield TN (1994) Potassium and incompatible-element enrichment in shoshonitic lavas from the Tavua Volcano, Fiji. Chem Geol 118: 43–62

Sack RO (1992) Thermochemistry of tetrahedrite–tennantite fahlores. In: *Price GD, Ross NL* (eds) Chapman and Hall, London, pp 243–266

Sack RO, Kuehner SM, Hardy LS (2002) Retrograde Ag-enrichment in fahlores from the Coeur d'Alene mining district, Idaho, USA. Mineral Mag 66: 215–229

Scherbarth NL, Spry PG (2000) Mineralogical and geochemical characteristics of the Tuvatu gold–silver telluride deposit, Upper Sabeto River, Fiji. In: *Bucci LA, Mair JL* (eds) Gold in 2000. Poster Session Extended Abstracts, Lake Tahoe, Nevada, November 10–11, 2000, pp 92–97

Setterfield TN, Eaton PC, Rose WJ, Sparks RSJ (1991) The Tavua Caldera, Fiji: a complex shoshonitic caldera formed by concurrent faulting and downsagging. J Geol Soc Lond 148: 115–127

Simon G, Kesler SE, Chryssoulis S (1999a) Geochemistry and textures of gold-bearing arsenian pyrite, Twin Creeks, Nevada: implications for deposition of gold in Carlin-type deposits. Econ Geol 94: 405–421

Simon G, Kesler SE, Russell N, Hall CM, Bell D, Pinero E (1999b) Epithermal gold mineralization in an old volcanic arc: the Jacinto deposit, Camaguey district, Cuba. Econ Geol 94: 487–506

Spry PG, Thieben SE (1996) Two new occurrences of benleonardite, a rare silver–tellurium sulphosalt, and a possible new occurrence of cervelleite. Mineral Mag 60: 871–876

Spry PG, Thieben SE (2000) The distribution and recovery of gold in the Golden Sunlight gold–silver telluride deposit, Montana, U.S.A. Mineral Mag 64: 31–42

Spry PG, Foster F, Truckle J, Chadwick TH (1997) The mineralogy of the Golden Sunlight gold–silver telluride deposit, Montana, U.S.A. Mineral Petrol 53: 143–164

Stanley CJ, Criddle AJ, Chisholm JE (1986) Benleonardite, a new mineral from the Bambolla mine, Moctezuma, Sonora, Mexico. Mineral Mag 50: 681–686

Stillwell FL (1949) Occurrence of tellurides at Vatukoula, Fiji. Proc Austral Inst Min Metall 154–155: 3–27

Stillwell FL, Edwards AB (1946) An occurrence of sub microscopic gold in the Dolphin East lode, Fiji. Proc Austral Inst Min Metall 141: 31–46

Stumpfl EF (1970) New electron probe and optical data on gold tellurides. Am Mineral 55: 808–815

Thompson TB, Trippel AD, Dwelley PC (1985) Mineralized veins and breccias of the Cripple Creek district, Colorado. Econ Geol 80: 1669–1688

Zhang X, Spry PG (1994a) Calculated stability of aqueous tellurium species, calaverite and hessite at elevated temperatures. Econ Geol 89: 1152–1166

Zhang X, Spry PG (1994b) Petrological, mineralogical, fluid inclusion, and stable isotope studies of the Gies gold–silver telluride deposit, Judith Mountains, Montana. Econ Geol 89: 602–627

Authors' address: *D. W. Pals* and *P. G. Spry* (corresponding author), Department of Geological and Atmospheric Sciences, 253 Science I, Iowa State University, Ames, Iowa 50011-3212, U.S.A., e-mail: pgspry@iastate.edu